

Error control in the numerical posterior distribution in the Bayesian UQ analysis of a semilinear evolution PDE

Maria L. Daza-Torres^{*§} J. Cricelio Montesinos-López[†]
 Marcos A. Capistrán[†] J. Andrés Christen[†] Heikki Haario[‡]

September 10, 2022

We elaborate on results obtained in [1] for controlling the numerical posterior error for Bayesian UQ problems, now considering forward maps arising from the solution of a semilinear evolution partial differential equation. Results in [1] demand an error estimate for the numerical solution of the FM. Our contribution is a numerical method for computing *after-the-fact* (ie *a posteriori*) error estimates for semilinear evolution PDEs, and show the potential applicability of [1] in this important wide range family of PDEs. Numerical examples are given to illustrate the efficiency of the proposed method, obtaining numerical posterior distributions for unknown parameters that are nearly identical to the corresponding theoretical posterior, by keeping their Bayes factor close to 1.

1 Introduction

A wide range of applications are concerned with the solution of an inverse problem (IP) [2, 3, 4, 5, 6, 7, 8]: given some observations of the output, $\mathbf{y} = (y_1, \dots, y_n)$, to determine the corresponding inputs θ such that

$$y_i = \mathcal{F}(\theta) + \text{error}.$$

We refer to the evaluation of \mathcal{F} as solving the forward problem and consequently \mathcal{F} is called the Forward Map (FM). In general, the FM is a complex non-linear map, with input parameters θ , defined by an initial/boundary value problem for a system of ordinary differential equation (ODE) or partial differential equation (PDE). Then, to evaluate $\mathcal{F}(\theta)$, we must solve an initial/boundary value problem for a system of (O, P)DEs.

^{*}Departamento de Matemáticas, CUCEI, Universidad de Guadalajara, Guadalajara, JAL, México. *mdaza-torres@cimat.mx*

[†]Centro de Investigación en Matemáticas (CIMAT), Jalisco S/N, Valenciana, Guanajuato, 36023, México. *jose.montesinos, marcos, jac at cimat.mx*

[‡]Lappeenranta University of Technology, Department of computational and process engineering, Lappeenranta, Finland and Finnish Meteorological Institute, Helsinki, Finland *heikki.haario@lut.fi*

[§]Corresponding author

IPs are typically ill-posed: there may be no solution, or the solution may not be unique and may depend sensitively on y_i [9]. A way to approach these difficulties is to formulate the IP in the Bayesian framework. Stuart [10] studied conditions for the well-posedness of the Bayesian formulation of IPs. In this scheme, a noise model is assumed for the observations, e.g.,

$$y_i = \mathcal{F}(\theta) + \varepsilon_i; \quad \varepsilon_i \sim \mathcal{N}(0, \sigma^2).$$

This observational model generate a probability density given the parameter θ , namely $P_{\mathbf{Y}|\Phi}(\mathbf{y}|\theta, \sigma)$, for fixed data \mathbf{y} , obtaining the likelihood function. Based on the available information, a prior model $P_{\Phi}(\cdot)$ is stated for $\Phi = (\theta, \sigma)$, and a posterior distribution is obtained,

$$P_{\Phi|\mathbf{Y}}(\theta, \sigma|\mathbf{y}) = \frac{P_{\mathbf{Y}|\Phi}(\mathbf{y}|\theta, \sigma) P_{\Phi}(\theta, \sigma)}{P_{\mathbf{Y}}(\mathbf{y})}.$$

However, the common denominator in Bayesian Uncertainty Quantification (UQ) of inverse problems is that we do not have an analytical or computationally precise and straightforward implementation of the FM. This necessarily involves a numerical approximation for the FM, $\mathcal{F}^{\alpha(n)}$, where $\alpha(n)$ represents a discretization used to approximate the FM, which leads to a numerical/approximate posterior distribution. Thus, the numerical solution of the model will then introduce some numerical error in the posterior. At least theoretically, the numerical errors in the FM can be controlled and reduced to an arbitrarily low level, by using finer discretizations, but what numerical error should be tolerated in the FM to obtain a correct and acceptable numeric posterior? That is, what is a correct numeric control in the perspective of the data and the prior distribution at hand.

Recently, the works [11, 1] have addressed the problem to control the numerical error induced in the posterior distribution, when not using the exact FM $\mathcal{F}(\theta)$ but instead $\mathcal{F}^{\alpha(n)}(\theta)$. The work [11] proposes the use of Bayes Factors to compare the approximate posterior distribution with the theoretical posterior, considering both as models for the available data. They show, for ODEs, that the Bayes factor (BF) of the theoretical posterior vs. the numeric posterior tends to 1 in the same order as the numerical solver used.

Later this idea was generalized in [1] to consider also PDEs and, more importantly, the use of the *expected* value of the BFs before observing data. This results in more practical and workable guidelines in a more realistic multidimensional setting. The main result in [1] is a bound on the absolute global error to be tolerated by the FM numerical solver, which guarantees that the resulting numerical posterior is indistinguishable from the theoretical posterior. The bound obtained allows deciding what precision to run the solver, which could require less computational effort. Indeed, a reliable estimate of the error for the numerical method used is the central point in the calculation of this bound.

Classical error estimates, both for finite differences and finite elements, are based on higher error bounds that have asymptotic convergence when the mesh size tends to zero. Unfortunately, these estimates imply “constants of stability” generally unknown and difficult to calculate. The

first papers to establish *after-the-fact* error estimates (ie. *a-posteriori* error estimates, we prefer to call then *after-the-fact* to avoid the obvious confusion with the Bayesian jargon), were published by Babuska and Rheinboldt in [12]. Currently, numerous works have been published trying to propose error estimators and computationally acceptable refinement strategies [13]. The work [14] presents a general approach to automated goal-oriented error control in the solution of nonlinear stationary finite element variational problems where local constants can be computed. In [15] the authors conclude that many error estimation techniques in practice do not provide mathematically proven limits on the error and should be used with care.

In this paper we derive after-the-fact numerical error estimates for physical models that involve a semi-linear evolution differential equation of the form

$$\frac{\partial u}{\partial t} = D \frac{\partial^2 u}{\partial x^2} + F\left(u, \frac{\partial u}{\partial x}, \theta\right), \quad (1)$$

defined on the region $t \in [0, \tau]$, $x \in [a, b]$, with left and right boundary conditions

$$u(a, t) = g(t) \quad \text{and} \quad u(b, t) = h(t), \quad 0 \leq t \leq \tau, \quad (2)$$

and initial condition $u(x, 0) = f(x)$, $a \leq x \leq b$. Here D is the diffusion coefficient, θ is a parameter (possibly a vector) of interest, and F is a non-linear operator.

This physical model arises in several fields of science and engineering [16, 17]. It is used to describe many complex nonlinear settings in applications such as vibration and wave propagation, fluid mechanics, plasma physics, quantum mechanics, nonlinear optics, solid state physics, chemical kinematics, physical chemistry, population dynamics and many other areas of mathematical modeling.

The numerical solution for Eq. (1) is obtained by discretizing first in the space with the finite difference (FD) method and solving the resulting system in time with the Runge-Kutta Cash-Karp (RKCK) method [18]. This scheme is widely used to solve numerically evolution partial differential equations [19, 20, 21]. However, numerical after-the-fact error estimates for these methods have not yet been derived.

The idea behind our construction of these error estimates for the PDE in Eq. (1) is the available error estimates for the RKCK method. Our numerical method uses these error estimates, in time, for the resulting ODE system. The truncated error introduced for the approximation with finite differences is computed using the solution in two different mesh sizes. In modern computers, the added computational effort can be hidden to result equivalent to solving the PDE conventionally (on a single mesh) since evaluating the solution in two different meshes may be easily parallelized.

We will use these after-the-fact error estimates in the solution of the Bayesian Inverse Problem (BIP) associated with the PDE given in Eq. (1). We assume data will be taken from observations at fixed points in space and at a given time, and unknown parameters (θ) will need to be recovered from Eq. (1) using a Bayesian approach.

For several examples, we show how our error estimation is applied to control the posterior distribution numerical error by maintaining the numerical error in $\mathcal{F}^{\alpha(n)}(\cdot)$ below the threshold recommended in [1], to obtain a posterior distribution nearly indistinguishable to the theoretical posterior distribution, if the theoretical solution of Eq. (1) would had been used. The results obtained show no differences between theoretical and numerical posterior and additional mesh refinements do not change the resulting posterior.

The outline of the rest of the paper is as follows. In Section 2 we present a numerical method that is used for solving numerically evolution partial differential equations. In Section 3 we derive our after-the-fact error estimates for semi-linear evolution differential equations. The accuracy of our error estimates is evaluated for some classic examples. In Section 4 we use this examples for defining corresponding BIP, and we show the performance of our error estimation in the application of the error control in the numerical posterior. Finally, in Section 5 a discussion of the our findings is provided.

2 Numerical Solution

Here we introduce a common numerical procedure for the solution of semilinear evolution partial differential equations. This procedure has been widely used for solving evolution partial differential equations [19, 20, 21]. The basic idea of the method is to replace the spatial derivation in the PDE with an algebraic approximation in order to obtain an ODE system. The resulting system is then solved with a standard ODE solver. We discretize in the space with the FD method and solving the ODE system with the RKCK method. We called to this method FD-RKCK.

For simplicity, we denote $\dot{u} := \frac{\partial u}{\partial t}$, $u' := \frac{\partial u}{\partial x}$, and $F(u, u')$ instead of $F(u, u', \theta)$. Moreover, without losing generality, we can set $D = 1$ in Eq. (1). We consider a one-dimensional uniform mesh on the region $[a, b]$, with nodes x_i , for $i = 0, 1, \dots, N$, where $a = x_0 < x_1 < \dots < x_N = b$, and a constant step size h between any two successive nodes, i.e., $h = x_i - x_{i-1}$.

To solve the PDE in Eq. (1) we start by linearizing F using the quasi-linearization method that was introduced in [19] for solving nonlinear evolution partial differential equations. This method consists in separating the function F into a linear (L) and a nonlinear (N) component, and rewrite the Eq. (1) in the form

$$\dot{u} = u'' + \mathbf{L}[u, u'] + \mathbf{N}[u, u']. \quad (3)$$

For example, in Section 3 we use the Fisher equation where $F = ru(1 - u)$, thus $\mathbf{L} = ru$ and $\mathbf{N} = -ru^2$. Afterwards, the nonlinear operator \mathbf{N} is approximated with a Taylor series, assuming that the difference $u_{i+1} - u_i$ and all its spatial derivatives are small, hence

$$\mathbf{N}[u_{i+1}, u'_{i+1}] \approx \mathbf{N}[u_i, u'_i] + \frac{\partial \mathbf{N}}{\partial u}[u_i, u'_i] \cdot (u_{i+1} - u_i) + \frac{\partial \mathbf{N}}{\partial u'}[u_i, u'_i] \cdot (u'_{i+1} - u'_i), \quad (4)$$

where $u_{i,\cdot} = u(x_i, t)$. Substituting Eq. (4) into Eq. (3), we get

$$\begin{aligned} \dot{u}_{i+1,\cdot} &= u''_{i+1,\cdot} + \mathbf{L}[u_{i+1,\cdot}, u'_{i+1,\cdot}] + \mathbf{N}[u_i, u'_{i,\cdot}] + \frac{\partial \mathbf{N}}{\partial u}[u_{i,\cdot}, u'_{i,\cdot}] \cdot (u_{i+1,\cdot} - u_{i,\cdot}) \\ &\quad + \frac{\partial \mathbf{N}}{\partial u'}[u_{i,\cdot}, u'_{i,\cdot}] \cdot (u'_{i+1,\cdot} - u'_{i,\cdot}), \end{aligned} \quad (5)$$

for $i = 1, \dots, N - 2$. Now, the spatial partial derivatives are approximated using the central difference formula. For simplicity, we use the simplest spatial derivative approximations here, while the analysis can be extended for other (e.g., five-point stencil) approximations as well,

$$u'_{i,\cdot} \approx \frac{u_{i+1,\cdot} - u_{i-1,\cdot}}{2h}, \quad u''_{i,\cdot} \approx \frac{u_{i+1,\cdot} - 2u_{i,\cdot} + u_{i-1,\cdot}}{h^2}, \quad (6)$$

for $i = 1, \dots, N - 1$, and

$$u'_{0,\cdot} \approx \frac{u_{1,\cdot} - u_{0,\cdot}}{h}. \quad (7)$$

Finally, substituting the approximate derivatives in Eqs. (6)–(7) into Eq. (5), jointed with the boundary condions given in Eq. (2), we get the following semi-discrete differential equation with a truncation error of order $O(h^p)$; $p = 1$ if \mathbf{N} is nonlinear in u' and $p = 2$ if \mathbf{N} is linear in u' :

$$\dot{\mathbf{U}} = \mathbf{A}_{xx} \mathbf{U} + \mathbf{F}(t, \mathbf{U}), \quad (8)$$

where $\mathbf{U} = (u_{1,\cdot}, u_{2,\cdot}, \dots, u_{N-1,\cdot})^T$,

$$\mathbf{A}_{xx} = \begin{pmatrix} -2 & 1 & 0 & \dots & 0 \\ 1 & -2 & 1 & \dots & \vdots \\ 0 & 1 & -2 & \dots & \vdots \\ \vdots & \vdots & \ddots & \ddots & 1 \\ 0 & \dots & 0 & 1 & -2 \end{pmatrix}_{(N-1) \times (N-1)}$$

and \mathbf{F} is the approximate operator F in matrix form.

In order to solve the resulting ODE system (8), with $N - 1$ equations, we use the RKCK method. This method uses six function evaluations to calculate fourth and fifth-order accurate solutions. The difference between these solutions is then taken to be the error (fourth order) of the solution (see details in [22]). The available error estimate is the motivation to solve the resulting ODE's system with this Runge-Kutta (RK) method, and it will be use in turn, in Section 3, for computing the global error of the numerical solution of Eq. (1).

Setting $\mathbf{G}(t, \mathbf{U}) = \mathbf{A}_{xx} \mathbf{U} + \mathbf{F}(t, U)$, a Runge-Kutta scheme applied to our model problem (8) can be written on the form

$$\begin{aligned}
\mathbf{K}_{1,n} &= \mathbf{G}(t_n, \mathbf{W}_{\cdot,n}), \\
\mathbf{K}_{l,n} &= \mathbf{G}\left(t_n + c_l k, \mathbf{W}_{\cdot,n} + k \sum_{j=1}^{l-1} a_{lj} \mathbf{K}_{j,n}\right), \quad l = 2, 3, \dots, 6, \\
\mathbf{W}_{\cdot,n+1} &= \mathbf{W}_{\cdot,n} + k \sum_{l=1}^6 b_l \mathbf{K}_{l,n},
\end{aligned}$$

where $\mathbf{W}_{\cdot,n+1}$ is the approximation for $\mathbf{U}(t_{n+1})$, (a_{lj}) are the Runge-Kutta coefficients, $\mathbf{b} = (b_1, b_2, \dots, b_6)$ are the quadrature nodes and $\mathbf{c} = (c_1, c_2, \dots, c_6)$ are the quadrature weights of the RK scheme. $k = \Delta t > 0$ is the step size in time defining a uniform grid, such that $t_{n+1} = t_n + k$.

Remark 1. To have stable solutions in explicit schemes, the step size in time is related to the discretization through the CFL condition [23], which restricts the step size in time based on the eigenspectrum of the discretized spatial operator. More precisely, the scheme is stable if only if the eigenspectrum of \mathbf{A} is less than zero, where \mathbf{A} is the discretized spatial operator. Computing the eigenvalues for the operator (1), following the scheme introduced in [22], we obtained the following stability condition on Δt ,

$$\frac{\Delta t D}{\Delta x^2} \leq \frac{1}{4} b_{max},$$

where $b_{max} = \max_i b_i$.

3 After-the-fact error estimates

In this section we propose a numerical procedure to obtain after-the-fact error estimates for the numerical solution of Eq. (1). For them, we use the error estimation in the time stepping given for the RKCK method and estimate the leading term of the truncation error in space stepping. This scheme can be extended for non-linear evolution differential equations, but some additional considerations about the stability of the solution must be taken care of.

Regarding the convergence order, in Section 2 we describe the numerical method used to solve the semi-discrete differential equation (8), with a truncation error of order p in space and fourth-order in time since the solution of this discrete system is approximated by the RKCK method. Therefore, overall the numerical solution of Eq. (1) has a truncation error of order $O(h^p + h^p k^4)$, that is, if we denote by $w_{i,n}$ the approximate solution of $u(x, t)$ at $x = x_i$ and $t = t_n$, we have that

$$u(x_i, t_n) = w_{i,n} + O(h^p + h^p k^4), \quad (9)$$

where $x_i = a + ih$, $i = 1 \dots, N - 1$, $t_n = nk$, $n = 1, \dots, M$.

Turning now to our after-the-fact error estimates, we need to characterize the error in the

solution resulting from the spatial and temporal discretization. From Eq. (9), the pointwise error can be written as

$$|u(x_i, t_n) - w_{i,n}| \leq C_1 h^p k^4 + C_2 h^p,$$

for some constants C_1 and C_2 . We are interested in the maximum absolute global error K (i.e., the maximum on the pointwise error);

$$K = \max_{i,n} |u(x_i, t_n) - w_{i,n}|. \quad (10)$$

Following, we propose an estimation for K . First, for h fixed, we compute an approximation for K using the error estimation given by the RKCK method; this approximation is of order $O(h^p k^4)$. Now, to compute the truncation error in the space, we use one technique commonly used, called step doubling. The idea is to calculate the solution using one step size h and then compute them again with half the space step ($h/2$). The result obtained using two steps size is more accurate than using the single-step size h . Their difference can, therefore, be used as an estimate of the truncation error, which in turn is proportional to the power of h .

Proposition 1. *Let $w_{i,n}$ the DF-RKCK approximation to the solution of the problem (1), at $x = x_i$ and $t = t_n$. The following after-the-fact error estimate is valid for a fixed h :*

$$\max_{i,n} |u(x_i, t_{n+1}) - w_{i,n+1}| \leq \left\| \sum_{j=1}^{n+1} k \left(\sum_{l=1}^s (\hat{b}_l - b_l) \mathbf{K}_{l,j} + Ch^p \right) \right\|_{\infty}, \quad (11)$$

for $i = 1, \dots, N-1$, $n = 1, \dots, M$, with C a constant.

Proof. For a fixed h , let $\mathbf{W}_{\cdot, n+1}$ and $\mathbf{Y}_{\cdot, n+1}$, the $n+1$ approximation of $\mathbf{U}_{\cdot, n+1}$ in system (8), of order 4 and 5 respectively, i.e,

$$\mathbf{W}_{\cdot, n+1} = \mathbf{W}_{\cdot, n} + k \left(\sum_{l=1}^s b_l \mathbf{K}_{l,n} + \mathbf{1} \cdot B_1 h^p \right)$$

and

$$\mathbf{Y}_{\cdot, n+1} = \mathbf{W}_{\cdot, n} + k \left(\sum_{l=1}^s \hat{b}_l \mathbf{K}_{l,n} + \mathbf{1} \cdot B_2 h^p \right),$$

for some constants B_1, B_2 . Here $\mathbf{1}$ denotes a vector of all ones. Now, the local truncation error at t_{n+1} for the RKCK method is given by

$$\tau_{\cdot, n+1} = k \left(\sum_{l=1}^s (\hat{b}_l - b_l) \mathbf{K}_{l,n} + \mathbf{1} \cdot (B_1 - B_2) h^p \right), \quad (12)$$

and the global truncation error estimator $\mathbf{e}_{n+1} = \mathbf{U}_{\cdot, n+1} - \mathbf{W}_{\cdot, n+1}$, at knot t_{n+1} , is defined as

follows:

$$\mathbf{e}_{n+1} := \sum_{j=1}^{n+1} \tau_{\cdot,j}. \quad (13)$$

Next, we take the maximum on \mathbf{e}_{n+1} joint with Eqs. (12)–(13), lead us

$$\max_{i,n} |u(x_i, t_{n+1}) - w_{i,n+1}| \leq \left\| \sum_{j=1}^{n+1} k \left(\sum_{l=1}^s (\hat{b}_l - b_l) \mathbf{K}_{l,j} + Ch^p \right) \right\|_{\infty},$$

for some constant C . \square

Now, we estimate the leading term of the truncation error in space stepping. We use that the solution of Eq. (1) can be written as follows,

$$u(x_i, t_n) \approx w_{i,n} + \hat{C}_1 h^p k^4 + \hat{C}_2 h^p.$$

Then, we compute the differences of two numerical solutions of $u(x, t)$: $w_{i,n}$ and $\tilde{w}_{i,n}$, for the step sizes h and $\tilde{h} = 2h$, respectively. Obtaining

$$\hat{C}_2 \tilde{h}^p - \hat{C}_2 h^p \approx (w_{2i,n} - \tilde{w}_{i,n}) + (\hat{C}_1 h^p k^4 - \hat{C}_1 \tilde{h}^p k^4),$$

for $i = 1, \dots, \frac{N-2}{2}$, $n = 1, \dots, M$. Now, taking the absolute value on both sides of the last equation and applying the triangle inequality, we have

$$\begin{aligned} \hat{C}_2 \left| \tilde{h}^p - h^p \right| &\leq |w_{2i,n} - \tilde{w}_{i,n}| + \left| \hat{C}_1 h^p k^4 - \hat{C}_1 \tilde{h}^p k^4 \right| \\ \hat{C}_2 &\leq \frac{|w_{2i,n} - \tilde{w}_{i,n}| + \left| \hat{C}_1 h^p k^4 - \hat{C}_1 \tilde{h}^p k^4 \right|}{\left| \tilde{h}^p - h^p \right|}. \end{aligned}$$

The above expression is valid for $i = 1, \dots, M$, then we take the maximum on i, n ,

$$\hat{C}_2 \leq \frac{\max_{i,n} |w_{2i,n} - \tilde{w}_{i,n}| + \left| \hat{C}_1 h^p k^4 - \hat{C}_1 \tilde{h}^p k^4 \right|}{h^p (2^p - 1)},$$

thus, we have found an upper approximation for C_2 , namely,

$$\tilde{C} \approx \frac{\max_{i,n} |w_{2i,n} - \tilde{w}_{i,n}| + \left| \hat{C}_1 h^p k^4 - \hat{C}_1 \tilde{h}^p k^4 \right|}{h^p (2^p - 1)},$$

then, the truncation error in h can be approximated as follows,

$$O(h^p) \approx \tilde{C}h^p. \quad (14)$$

Remark 2. From Proposition 1 and Eq. (14), an after-the-fact error estimate to the DF-RKCK method to the solution of the problem (1) is given by

$$\max_{i,n} |u(x_i, t_{n+1}) - w_{i,n+1}| \leq \left\| \sum_{j=1}^{n+1} k \left(\sum_{l=1}^s (\hat{b}_l - b_l) \mathbf{K}_{l,j} + Ch^p \right) \right\|_{\infty} + \tilde{C}h^p, \quad (15)$$

we called the right side the above inequality \hat{K} .

In Algorithm 1, we describe in detail the steps necessary to compute the numerical solution of Eq. (1), with the after-the-fact error estimation, \hat{K} , just explained. We call this algorithm DF-RKCK.

To test our algorithm we consider three classical semi-linear PDEs, of the form (1): Example 1 (Fisher equation), Example 2 (Fitzhugh-Nagumo equation), and Example 3 (Burgers-Fisher equation). The three examples used also have analytic solutions, allowing us to compute the actual numerical error and compare it with our estimates. In Figure 1, a graphical comparison is shown between our numerical implementation approximations and the exact solution for the three examples. Table 1 shows the convergences order of the solution obtained with the DF-RKCK Algorithm. It can be seen that the method achieves full convergence for the error (order 2) for Examples 1 and 2, but the order of convergence for Example 3 is 1, and this is due to the non-linearity of F in u' , as was mentioned before.

Remark 3. To compute the numerical convergence rate, we use

$$p = \log_2 \left(\frac{\|u_{4h} - u_{2h}\|_{\infty}}{\|u_{2h} - u_h\|_{\infty}} \right).$$

h	Example 1	Example 2	Example 3
0.0125	1.999092	1.992578	1.075049
0.0083	1.999617	1.995410	1.052625
0.00625	1.999789	1.996692	1.040450
0.005	1.999866	1.997418	1.032826

Table (1) The convergence rate of the DF-RKCK method.

In Figure 2 we show the maximum error between the exact solution and the numerical solution for the three examples considered, comparing it to our error estimates. We can see that the estimation proposed for the absolute global error is an upper bound for the exact error. The

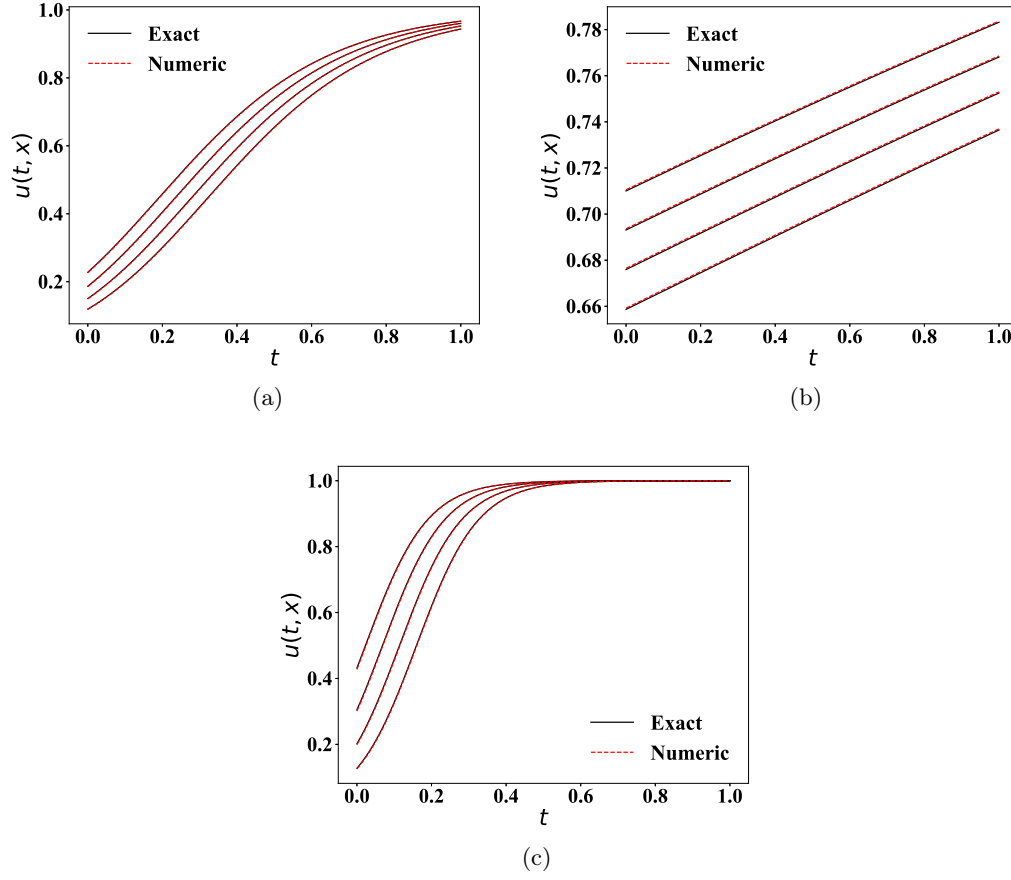


Figure (1) The analytical and approximate solution in $x = 0.1, 0.3, 0.5, 0.7$, with step sizes in space $h = 0.0125$ and in time $k = 0.0001$, for: (a) the Fisher's equation, (b) the Fitzhugh-Nagumo equation, and (c) the Burgers-Fisher equation.

numerical implementation has been performed in Python, using the scipy, numpy and matplotlib packages. For the sake of reproducibility, all code is available in a Github repository [24].

Example 1 (Fisher equation). Fisher's equation belongs to the class of reaction-diffusion equation and is encountered in chemical kinetics and population dynamics applications. The equation is given by

$$\frac{\partial u}{\partial t} = \frac{\partial^2 u}{\partial x^2} + ru(1 - u), \quad (17)$$

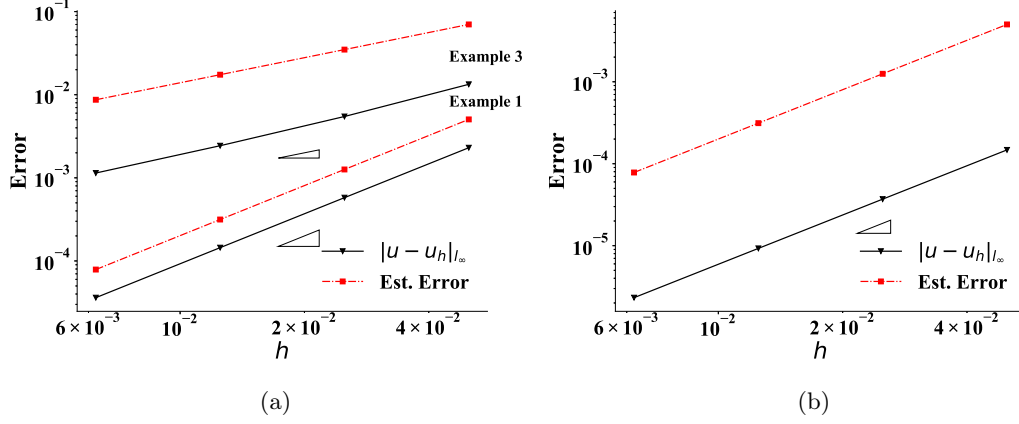


Figure (2) The maximum error between the exact solution and our DF-RKCK method against the error estimation: (a) the Fisher and the Burgers-Fisher equation, (b) the Fitzhugh-Nagumo equation. Different step sizes (h) in space are taken and for time we let $k = \alpha h^2$, with $\alpha = 3/4$.

with boundary and initial conditions

$$\begin{aligned} u(0, t) &= \frac{1}{(1 + e^{-5t})^2}, \quad 0 \leq t \leq \tau, \\ u(1, t) &= \frac{1}{(1 + e^{1-5t})^2}, \quad 0 \leq t \leq \tau, \\ u(x, 0) &= \frac{1}{(1 + e^x)^2}, \quad 0 \leq x \leq 1. \end{aligned}$$

This PDE has the following analytic close form solution

$$u(x, t) = \frac{1}{[1 + \exp(\sqrt{\frac{r}{6}}x - \frac{5r}{6}t)]^2}, \quad x \in [0, 1], \quad \text{and} \quad t \in [0, \tau],$$

where r is a parameter. The non-linear operator is $F(u, u', r) = ru(1-u)$; hence the appropriate linear component is $\mathbf{L} = ru$ and the nonlinear component is $\mathbf{N} = -ru^2$; we see that the operator F does not depend on u' so the method achieves order 2, as can be seen in Table 1. For the examples in Figs. (1)–(2) and Table 1 we use $r = 4$ and this parameter will be tried to identify using synthetic data in section 4.

Example 2 (Fitzhugh-Nagumo equation). The Fitzhugh-Nagumo equation is given by

$$\frac{\partial u}{\partial t} = \frac{\partial^2 u}{\partial x^2} + u(1-u)(u-a), \quad 0 < a < 1, \quad (18)$$

with boundary and initial conditions

$$\begin{aligned} u(0, t) &= \frac{1}{2}(1+a) + \frac{1}{2}(1-a) \tanh\left(\frac{(1-a^2)}{4}t\right), \quad 0 \leq t \leq \tau, \\ u(1, t) &= \frac{1}{2}(1+a) + \frac{1}{2}(1-a) \tanh\left(\sqrt{2}(1-a)\frac{1}{4} + \frac{(1-a^2)}{4}t\right), \quad 0 \leq t \leq \tau, \\ u(x, 0) &= \frac{1}{2}(1+a) + \frac{1}{2}(1-a) \tanh\left(\sqrt{2}(1-a)\frac{x}{4}\right), \quad 0 \leq x \leq 1. \end{aligned}$$

The analytic solution for this PDE is given by

$$u(x, t) = \frac{1}{2}(1+a) + \frac{1}{2}(1-a) \tanh\left(\sqrt{2}(1-a)\frac{x}{4} + \frac{(1-a^2)}{4}t\right), \quad x \in [0, 1], \quad \text{and} \quad t \in [0, \tau],$$

where a is a parameter. The non-linear operator is $F(u, u', a) = u(1-u)(u-a)$; hence the appropriate linear component is $\mathbf{L} = -au$ and the nonlinear component is $\mathbf{N} = u^2(1-u+a)$; we see that the operator F does not depend on u' so the method achieves order 2, as can be seen in Table 1. For the examples in Figs. (1)–(2) and Table 1 we use $a = 0.3$ and this parameter will be tried to identify using synthetic data in section 4.

Example 3 (Burgers-Fisher equation). The Burgers-Fisher equation is given by

$$\frac{\partial u}{\partial t} = \frac{\partial^2 u}{\partial x^2} - ruu' + su(1-u), \quad (19)$$

with the initial condition

$$u(x, 0) = \frac{1}{2} + \frac{1}{2} \tanh\left(-\frac{r}{4}x\right), \quad 0 \leq x \leq 1,$$

and with boundary and initial conditions

$$\begin{aligned} u(0, t) &= \frac{1}{2} + \frac{1}{2} \tanh\left(\left(\frac{r^2}{8} + \frac{s}{2}\right)t\right), \quad 0 \leq t \leq \tau, \\ u(1, t) &= \frac{1}{2} + \frac{1}{2} \tanh\left(-\frac{r}{4}\left[1 - \left(\frac{r}{2} + \frac{2s}{r}\right)t\right]\right), \quad 0 \leq t \leq \tau, \\ u(x, 0) &= \frac{1}{2} + \frac{1}{2} \tanh\left(-\frac{r}{4}x\right), \quad 0 \leq x \leq 1. \end{aligned}$$

This problem also has an analytic solution given by

$$u(x, t) = \frac{1}{2} + \frac{1}{2} \tanh\left(-\frac{r}{4}\left[x - \left(\frac{r}{2} + \frac{2s}{r}\right)t\right]\right), \quad x \in [0, 1], \quad \text{and} \quad t \in [0, \tau],$$

where r and s are parameters. The non-linear operator is $F(u, u', a) = -ruu' + su(1-u)$; hence the appropriate linear component is $\mathbf{L} = su$ and the nonlinear component is $\mathbf{N} = -ruu' - su^2$. Of note is that the order of convergence for the error is 1 because F is nonlinear in u' . For the

examples in Figs. (1)–(2) and Table 1 we use $r = 4.5$ and $s = 5.5$, and this parameters will be tried to identify using synthetic data in the next section.

4 Inverse Problem

In this section the numerical error estimation, proposed in Section 3 for the FM, is used to control the error in the numerical posterior. We use the three previous examples presented in Section 3 to illustrate the performance of the error estimation in the solution of the corresponding BIP, using simulated data sets.

We simulate data as follows. The (synthetic) observations, $\mathbf{y} = (y_1, \dots, y_n)$, are generated under model

$$y_i = \mathcal{F}_j(\theta) + \varepsilon_i, \quad (20)$$

where ε_i are independent and identically distributed as $\mathcal{N}(0, \sigma^2)$, $\theta \in \Theta \subset \mathbb{R}^d$ is a vector of unknown parameters, and $\mathcal{F}_j(\theta)$ represent the FM. In all our examples we consider the variance σ^2 to be known.

Equation (1) with its initial and boundary conditions define our FM. We consider the BIP to estimate the parameter θ given observations $\mathcal{F}_j(\theta) = u(x_j, t_1, \theta)$ at some points in space x_j , for $j = 1, 2, \dots, n$ and at a fixed time $0 < t_1 \leq \tau$. That is, we let the system to evolve until time t_1 and then observe it at the spacial locations x_j 's. The resulting observations are $y_j = u(x_j, t_1, \theta) + \varepsilon_i; \varepsilon_i \sim \mathcal{N}(0, \sigma^2)$.

The IP will be treated as a statistical inference problem under a Bayesian approach, setting a prior distribution $\pi_\Theta(\theta)$ on the unknown parameters to obtain the posterior distribution $\pi_{\Theta|Y}(\theta|y)$, from which all required inferences are drawn [10]. Implementation was done using Markov Chain Monte Carlo (MCMC) through a generic MCMC algorithm called the t-walk [25].

To control the error in the numerical posterior we follow the strategy of [1], where a bound is provided for the maximum error in the FM that depends on the sample size n and the standard deviation σ . The idea is to keep the *Expected Absolute Bayes Factor* (EABF) below a small threshold (e.g. $\frac{1}{20}$), so that the Bayes Factor between the theoretical and the numeric posteriors is close to 1. Assuming Gaussian independent data and letting the $\text{EABF} \leq b$, it is required that $\sqrt{\frac{1}{2\pi}} \frac{n}{\sigma} K < b$, see [1] for details. That is, we need that the numerical error (K) in the FM satisfies

$$K < b \frac{\sigma}{n} \sqrt{2\pi}, \quad (21)$$

where (σ) is the standard error in the model (20) and (n) is the sample size. Suppose we have an algorithm to simulate from posterior distribution, the Algorithm 2 describes a strategy to incorporate the bound (21) to control the error in the posterior distribution.

The basic idea of Algorithm 2 is to start with a relatively large step size (e.g., $h = 0.1$) and the step size in time is established to keep the stability condition $k = \frac{3}{4}h^2$. At each iteration of the MCMC, the FM, $\mathcal{F}^{h,k}(\cdot)$, is first computed along with its error estimation \hat{K} , using

Algorithm 1. If the solution u_h do not satisfy (21), a new solution is attempted by reducing the spatial step size by half and the step size in time is $k = \alpha h^2$, until (21) is satisfied.

Example 4 (Inverse Problem - Fisher's equation). We consider the BIP to estimate $\theta = r$ in the Fisher's equation of Example 1, given measurements of $\mathcal{F}_j(\theta)$ at time $t_1 = 0.4$. The synthetic data are simulated with the error model (20) and the following parameters: $\theta = 4$ and $\sigma = 0.007$, to maintain a 0.01 signal-to-noise ratio. The Eq. (17) with the initial and boundary conditions define our FM. We consider $n = 8$ observations at locations x_i regularly spaced between 0 and 1. The data are plotted in Fig. 3 (a).

Considering a tolerance $b = \frac{1}{20}$ in (21) and with the standard error and sample size used, calculating the error bound for the FM as stated in [1], to obtain the bound $B := b \frac{\sigma}{m} \sqrt{2\pi} = 1.1 \times 10^{-4}$. We require a prior distribution, $\pi(\cdot)$, for the parameter θ ; it is assumed that $\theta \sim \text{Gamma}(\alpha_1, \beta_1)$ with hyperparameters all known. Regarding the numerical solver, we begin with a relatively large step size $h = 0.05$ and the step size in time is established to keep the stability condition $k = \frac{3}{4}h^2$. After this, we start the Algorithm 2. For $h = 0.01$, the bound B is achieved for all iterations.

We compare the posterior distributions using the numerical FM vs. the exact FM, with 200,000 iterations of the t-walk; the histograms is reported with 150,000 samples, since the first 50,000 are discarded as burn-in. The results are shown in Fig. 3 (b). The small differences observed in both results may be attributed to the effect of generating approximate samples from the posterior distribution by use of MCMC methods.

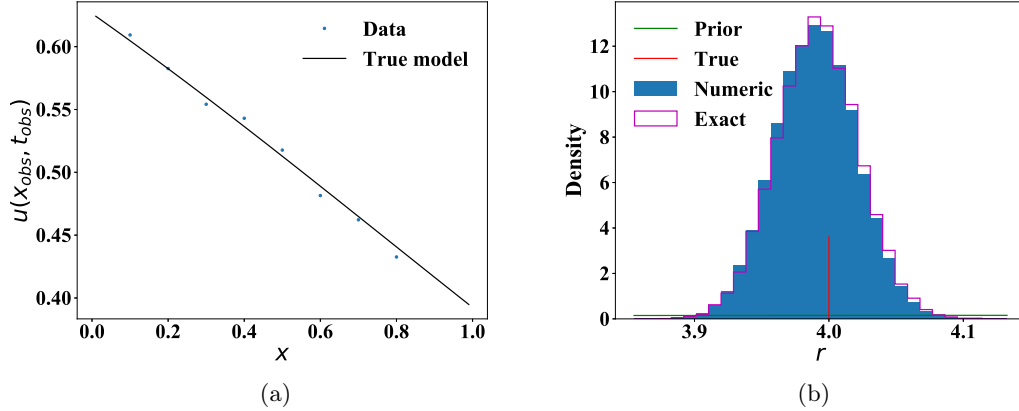


Figure (3) (a) Fisher equation example data (blue points) and true model (black line), considering $r = 4$. (b) Comparison between numerical (blue) and theoretical (magenta) posterior for parameter r . The green line represent the prior distribution.

Example 5 (Fitzhugh-Nagumo equation). For this example, the IP is to estimate $\theta = a$ in the Fitzhugh-Nagumo equation of Example 2, given measurements $\mathcal{F}_j(\theta)$ at time $t_1 = 0.4$. The synthetic data are simulated with the error model (20) and the following parameters: $\theta = 0.3$ and $\sigma = 0.007$; the Eq. (18) with the initial and boundary conditions define our FM. We consider

$n = 8$ observations at locations x_i regularly spaced between 0 and 1. The data are plotted in Fig. 4 (a).

To be able to get the posterior distributions, we assume that $\theta \sim \text{Gamma}(\alpha_2, \beta_2)$ with hyperparameters all known. With the standard error and sample size used, considering a tolerance $b = \frac{1}{20}$ in (21), calculating the error bound for the FM, getting $B = 1.1 \times 10^{-4}$. Regarding the numerical solver, we begin with a step size $h = 0.1$ and the step size in time $k = \frac{3}{4}h^2$. After this we start the Algorithm 2; for $h = 0.0125$, the bound is achieved for all iterations.

We compare the posterior distributions using the numerical FM vs. the exact FM, with 200,000 iterations of the twalk; the histograms is reported with 150,000 samples, since the first 50,000 are discarded as burn-in. The results are shown in Fig. 4 (b).

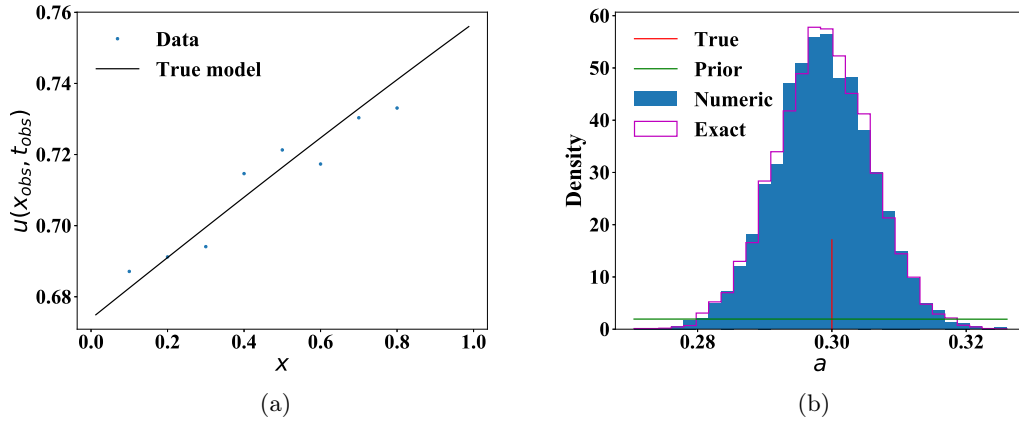


Figure (4) (a) Fitzhugh-Nagumo equation example data (blue points) and true model (black line), considering $a = 0.3$. (b) Comparison between numerical (blue) and theoretical (magenta) posterior for parameter a . The green line represent the prior distribution.

Example 6 (Burgers-Fisher equation). For this example, the IP is to estimate $\theta = (r, s)$ in the Burgers-Fisher equation of Example 4, given measurements $\mathcal{F}_j(\theta)$ at time $t_1 = 0.2$. The synthetic data are simulated with the error model (20) and the following parameters: $\theta = (4.5, 5.5)$ and $\sigma = 0.05$. The Eq. (19) with the initial and boundary conditions define our FM. We consider $n = 10$ observations at locations x_i regularly spaced between 0 and 1, and at time $t_1 = 0.3$. The data are plotted in Fig.5 (a).

To be able to get the posterior distributions, we assume independent priors between the parameters of the model. We assume that $r \sim \text{Gamma}(\alpha_r, \beta_r)$ and $s \sim \text{Gamma}(\alpha_s, \beta_s)$ with hyperparameters all known. With the standard error and sample size used, considering a tolerance $b = \frac{1}{20}$ in (21), calculating the error bound for the FM, getting $B = 6 \times 10^{-4}$. Regarding the numerical solver, we begin with a step size $h = 0.1$ and the step size in time $k = \frac{3}{4}h^2$. After this we start the Algorithm 2; for $h = 0.0017$, the bound is achieved for all iterations.

We compare the posterior distributions using the numerical FM vs. the exact FM, with 200,000 iterations of the twalk; the histograms is reported with 150,000 samples, since the first

50,000 are discarded as burn-in. The results are shown in Fig. 5 (b)–(c).

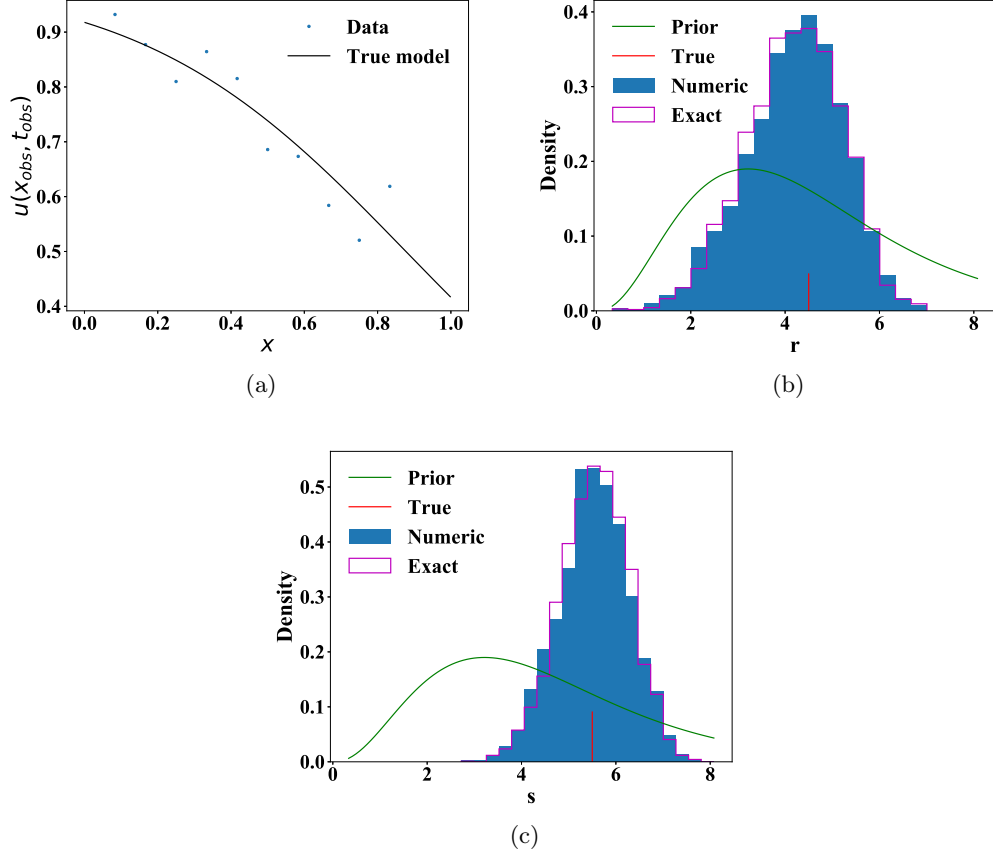


Figure (5) (a) Burgers-Fisher equation example data (blue points) and true model (black line), considering $\theta = (4.5, 5.5)$. Histogram from the numerical (blue) and theoretical (magenta) posterior distribution for: (b) parameter r and (c) parameter s . The green line represent the prior distribution.

5 Conclusions

In this paper, we proposed an error estimation for a class partial differential equations motivated by its application in the uncertainty quantification area. Our error estimation allows us to apply the results obtained in [1] for controlling the error in the respective numerical posterior for inverse problems that the forward mapping involve a semi-linear evolution PDE.

We presented three workout examples; in all cases, the numerical error in the posterior was successfully controlled, which led to a negligible increase in accuracy if the exact FM is considered. This, in turn, may result in CPU time save, as cheaper/rougher solvers are used.

Although two numerical solutions are required for the error estimation, the added computational effort can be hidden to result equivalent to solving the PDE conventionally (on a single

mesh) since evaluating the solution in two different meshes may be easily parallelized.

For future work, we plan to extend the method used for computing the error estimation to nonlinear evolution differential equations, but some consideration about the stability of the solution needs to be added and the convergence orders.

Acknowledgements

MLDT, JCML, MAC and JAC are partially funded by CONACyT CB-2016-01-284451, RDE-COMM and ONRG grants. JCML thanks CONACyT for his PhD scholarship at CIMAT. HH was funded by The Academy of Finland Centre of Excellence of Inverse Modelling and Imaging, decision number 312122.

References

- [1] J. A. Christen, M. A. Capistrán, M. L. Daza-Torres, H. Flores-Argüedas, and J. Cricelio Montesinos-López. Posterior distribution existence and error control in Banach spaces in the Bayesian approach to UQ in inverse problems. Technical Report 1712.03299, arXiv, October 2018.
- [2] Jari P Kaipio and Colin Fox. The bayesian framework for inverse problems in heat transfer. *Heat Transfer Engineering*, 32(9):718–753, 2011.
- [3] Caifang Cai, All Mohammad-Djafari, Samuel Legoupil, and Thomas Rodet. Bayesian data fusion and inversion in x-ray multi-energy computed tomography. In *2011 18th IEEE International Conference on Image Processing*, pages 1377–1380. IEEE, 2011.
- [4] Khosrow Chadán, David Colton, Lassi Päiväranta, and William Rundell. *An introduction to inverse scattering and inverse spectral problems*. SIAM, 1997.
- [5] David S Holder. *Electrical impedance tomography: methods, history and applications*. CRC Press, 2004.
- [6] OR Burggraf. An exact solution of the inverse problem in heat conduction theory and applications. *Journal of Heat transfer*, 86(3):373–380, 1964.
- [7] Roel Snieder and Jeannot Trampert. Inverse problems in geophysics. In *Wavefield inversion*, pages 119–190. Springer, 1999.
- [8] Maria L Daza, Marcos A Capistrán, J Andrés Christen, and Lili Guadarrama. Solution of the inverse scattering problem from inhomogeneous media using affine invariant sampling. *Mathematical Methods in the Applied Sciences*, 40(9):3311–3319, 2017.
- [9] Jari Kaipio and Erkki Somersalo. *Statistical and computational inverse problems*, volume 160. Springer Science & Business Media, 2005.

- [10] Andrew M Stuart. Inverse problems: a bayesian perspective. *Acta numerica*, 19:451–559, 2010.
- [11] M. Capistrán, J.A. Christen, and S. Donnet. Bayesian Analysis of ODE’s: solver optimal accuracy and Bayes factors. *Journal of Uncertainty Quantification*, 4(1):829–849, 2016.
- [12] Ivo Babuška and Werner C Rheinboldt. A-posteriori error estimates for the finite element method. *International Journal for Numerical Methods in Engineering*, 12(10):1597–1615, 1978.
- [13] Mats G Larson and Fredrik Bengzon. The finite element method: theory, implementation, and practice. *Texts in Computational Science and Engineering*, 10, 2010.
- [14] Marie E Rognes and Anders Logg. Automated goal-oriented error control i: Stationary variational problems. *SIAM Journal on Scientific Computing*, 35(3):C173–C193, 2013.
- [15] Thomas Grätsch and Klaus-Jürgen Bathe. A posteriori error estimation techniques in practical finite element analysis. *Computers & structures*, 83(4-5):235–265, 2005.
- [16] Spyros G Tzafestas. *Distributed parameter control systems: Theory and application*, volume 6. Elsevier, 2013.
- [17] Toka Diagana. *Semilinear Evolution Equations and Their Applications*. Springer, 2018.
- [18] Jeff R Cash and Alan H Karp. A variable order runge-kutta method for initial value problems with rapidly varying right-hand sides. *ACM Transactions on Mathematical Software (TOMS)*, 16(3):201–222, 1990.
- [19] PG Dlamini and M Khumalo. A new compact finite difference quasilinearization method for nonlinear evolution partial differential equations. *Open Mathematics*, 15(1):1450–1462, 2017.
- [20] Mehdi Bastani and Davod Khojasteh Salkuyeh. A highly accurate method to solve fisher’s equation. *Pramana*, 78(3):335–346, 2012.
- [21] Murat Sari and Gürhan Gürarslan. A sixth-order compact finite difference method for the one-dimensional sine-gordon equation. *International Journal for Numerical Methods in Biomedical Engineering*, 27(7):1126–1138, 2011.
- [22] Richard L Burden and J Douglas Faires. *Numerical analysis (ed.)*. Brooks/Cole, 2000.
- [23] Richard Courant, Kurt Friedrichs, and Hans Lewy. Über die partiellen differenzengleichungen der mathematischen physik. *Mathematische annalen*, 100(1):32–74, 1928.
- [24] See supplemental material at <https://github.com/mdazatorres> for the python codes.
- [25] J Andrés Christen, Colin Fox, et al. A general purpose sampling algorithm for continuous distributions (the t-walk). *Bayesian Analysis*, 5(2):263–281, 2010.

Algorithm 1 DF-RKCK

Step 1: Initialization:

- Spatial step size h , the step size in time is given for keeping the stability condition $k = \alpha h^2$
- Initial condition W_0 ; initial time t_0 ; parameter θ . Set $\hat{C}_1 = 1$
- The RK matrix $\mathbf{A} = (a_{ij})$, the nodes $\mathbf{b} = (b_1, b_2, \dots, b_6)$ and the weights $\mathbf{c} = (c_1, c_2, \dots, c_6)$

Step 2. Discretizing (1) with the FD method for h , as is described in Section 2:

$$\dot{\mathbf{U}} = \mathbf{F}(\mathbf{U}) \quad (16)$$

Step 3. Solve (16) with the Cash-Karp method:

For $n = 1, 2, \dots, M$:

Step 4. For $i = 2, 3, \dots, 6$:

$$\begin{aligned} \mathbf{K}_1 &= \mathbf{G}(t_n, \mathbf{W}_{\cdot, n}) \\ \mathbf{K}_i &= \mathbf{G}\left(t_n + c_i k, \mathbf{W}_{\cdot, n} + k \sum_{j=1}^{i-1} a_{ij} \mathbf{K}_j\right) \end{aligned}$$

Step 5. Compute

$$\begin{aligned} \mathbf{W}_{\cdot, n+1} &= \mathbf{W}_{\cdot, n} + k \sum_{i=1}^6 b_i \mathbf{K}_i \\ \mathbf{E}_{\cdot, n+1} &= \mathbf{E}_{\cdot, n} + k \left(\sum_{i=1}^6 (b_i - \hat{b}_i) \mathbf{K}_i + h^p \right) \end{aligned}$$

Step 6. Take $\epsilon_1^{h,k} = \hat{C}_1 \|\mathbf{E}_{\cdot, M+1}\|_\infty$

Step 7. Output: $\mathbf{W}^{h,k}, \epsilon_1^{h,k}$

Step 8. Repeat the Step 2 - 7, for the step size $2h$

Step 9. Compute \hat{C}_2

$$\hat{C}_2 = \left(\|\mathbf{W}^{h,k} - \mathbf{W}^{2h,k}\|_{l_\infty} + \left| \epsilon_1^{h,k} - \epsilon_1^{2h,k} \right| \right) / (h^p (2^p - 1))$$

Step 10. Compute ϵ_2 , ($\epsilon_2^{h,k} = \hat{C}_2 h^p$)

Step 11. Compute the error in the solution approximated $\mathbf{W}^{h,k}$,

$$\hat{K}^{h,k} = \epsilon_1^{h,k} + \epsilon_2^{h,k}$$

Step 12: Output: $\mathbf{W}^{h,k}, \hat{K}^{h,k}$

Algorithm 2 Numerical refinement for FM in the MCMC algorithm

- Spatial step size h (large)
- Standard error (σ) and sample size (n)
- Calculate the error bound $B = b \frac{\sigma}{n} \sqrt{2\pi}$ with a tolerance b , we suggest $b = \frac{1}{20}$
- Initial value for the parameter, θ^0
- MCMC length M (number of simulations)

Step 2. For $i = 1, 2, \dots, M$:

Step 3. Compute the FM, $\mathcal{F}^h(\theta^{i-1})$, along with its error estimation $\hat{K}^{h, \theta^{i-1}}$, using Algorithm 1

Step 4. If $\hat{K}^{h, \theta^{i-1}} > B$

- Set $h = h/2$

- Return to *Step 3*

Else

- Simulate θ^i with some MCMC algorithm

Step 5: Output: $(\theta^0, \theta^1, \dots, \theta^M)$
